

Texture, structure and phase transformation in sputter beta tantalum coating

S.L. Lee*, M. Doxbeck, J. Mueller, M. Cipollo, P. Cote

US Army Armament Research, Development and Engineering Center, Benét Labs, Waterlout, NY 12189-4050, USA

Abstract

Structural properties of tantalum are of interest because of its potential application in high temperature wear and erosion. In this paper, we report on beta tantalum coatings, which were sputter-deposited onto inner surface of steel cylinders, and flat steel and glass plates. Two forms of beta tantalum coatings were generally observed: high (002) fiber-texture at low sputter gas pressure, and more random oriented beta tantalum at higher sputter gas pressure. Two-dimensional XRD and pole figure analyses showed both belong to the same tetragonal structure. Structure simulation was made using a tetragonal cell, $a=1.0194$ nm, $c=0.5313$ nm, space group $P4_2/mnm$ and a very similar cell, $a=1.0211$ nm, $c=0.53064$ nm, space group $P-421m$ by Frank–Kasper (1958, 1959) and Arakcheeva (2002). Diffraction pattern generated using the former space group allows (00 l) reflections for even l , while the latter allows both even and odd (00 l) reflections. The latter model provides better interpretation of our data. Upon annealing, the (002) grains in random oriented tantalum became unstable at 300 °C, and complete beta to alpha tantalum phase transformation occurred at ~ 750 °C, resulting in alpha tantalum with (110) preferred orientation. In highly textured (002) beta tantalum, hot hardness measurements showed hardness decreased drastically between 250 and 350 °C to hardness values of alpha tantalum, suggesting a phase transformation approximately 300 °C. XRD data showed partial beta to alpha phase transformation and re-orientation of the (002)-grains at 100 °C, and was more intense at 300 °C.

© 2003 Elsevier B.V. All rights reserved.

Keywords: Beta tantalum; Tetragonal tantalum; Magnetron sputter deposition; Structure; Texture; Phase transformation; Hot hardness

1. Introduction

Tantalum is of technical interest because of its importance in electronics, X-ray optics and high temperature wear and erosion. Properties of alpha and beta tantalum are listed in Table 1. Bulk tantalum exists in bcc structure, also known as alpha tantalum. However, magnetron sputtering, chemical vapor deposition and electrochemical deposition in eutectic molten salt solution can produce both single and mixed phases of bcc alpha and tetragonal beta tantalum.

Tantalum as a diffusion barrier material between Cu and Si has been reported [1–5]. Potential applications of tantalum as protective bore coatings have been reported [6–11]. Real-time XRD techniques have been developed to study phase evolution in sputtered tantalum films [11–14]. Clevenger [4] found intrinsic compressive

stress relief accompanied beta to alpha phase transition of tantalum. Latt et al. [5] investigated Cu penetration, oxidation, phase transformation in thermal annealing of multi-layers containing tantalum. Hoogveen [15] studied epitaxial growth of tantalum on aluminum, and reported that the beta to alpha phase transformation temperature was dependent on tantalum layer thickness. Liu et al. [16] studied annealing effects of tantalum films on Si, including increasing oxygen content and compressive stresses. Klaver [17] performed molecular dynamics simulation of the growth of bcc and beta tantalum, thermal stability of beta tantalum, and reported cohesion energy in beta tantalum less than in bcc tantalum.

Read [18] discovered beta tantalum and suggested a tetragonal structure $a=0.534$ nm, $c=0.994$ nm. Given that beta tantalum and beta uranium are isomorphous, Donohue [19] and Lawson [20] investigated $P4_2/mnm$, $P4_2/nm$ and $P-4n2$ space groups for beta uranium. Moseley [21] obtained single-phase beta tantalum from electrolytic deposition in molten salt, and indexed it

*Corresponding author. Tel.: +1-518-266-5503; fax: +1-518-266-4661.

E-mail address: sabrilee@pica.army.mil (S.L. Lee).

Table 1
Thermal–mechanical properties of alpha and beta tantalum

Phase	Alpha tantalum	Beta tantalum
Structure	BCC, S.G. Im3m	Tetragonal, S.G. $P4_2/mnm$
Lattice parameters	$a=b=c=0.33058$ nm	$a=b=1.0194$ nm, $c=0.5313$ nm
Hardness	200–400 KHN	1000–1300 KHN
Ductility	Ductile	Brittle
Resistivity	15–60 $\mu\Omega$ cm	170–210 $\mu\Omega$ cm
Thermal stability	$T_{\text{Melting point}}$ at 2996 °C	$T_{\text{Beta-alpha}}$ at 750–775 °C

Table 2
Deposition conditions of selected beta tantalum specimens from a cylindrical magnetron, a conventional, and an in-situ sputtering system with real-time XRD

Specimen	Press Pa (mTorr)	Substrate	Sputter system	Gas	Thick (μm)	Surface texture
Kr1 (1-10815)	0.26 (2)	Steel cylinder	Cylindrical	Kr	66	(002) Textured
Kr2 (8-000609)	1.3 (10)	Steel cylinder	Cylindrical	Kr	120	(002) Textured
Kr3 (6-000504)	3.3 (25)	Steel cylinder	Cylindrical	Kr	120	Random
Kr4 (4-00029)	3.9 (30)	Steel cylinder	Cylindrical	Kr	30	Random
Kr5 (11-00728)	13 (100)	Steel cylinder	Cylindrical	Kr	20	Random
Ar1 (Tasteel)	1.3 (10)	Steel plate	Planar	Ar	50	(002) Textured
Ar2 (Taglass)	1.3 (10)	Glass plate	Planar	Ar	50	(002) Textured
Ar3 (In-situ-1)	1.3 (10)	Steel plate	In-situ planar	Ar	0.65	(002) Textured
Ar4 (In-situ-2)	2.6 (20)	Steel plate	In-situ planar	Ar	0.51	Less random
Ar5 (In-situ-3)	3.9 (30)	Steel plate	In-situ planar	Ar	0.47	More random
Ar6 (In-situ-4)	5.2 (40)	Steel plate	In-situ planar	Ar	0.34	Random
Ar7 (80915)	9.1 (70)	Steel cylinder	Cylindrical	Ar	120	Random

using a tetragonal cell $a=1.0194$ nm, $c=0.5313$ nm, S.G. $P4_2/mnm$. ICDD [22] replaced Read's [18] cell (19-1290) with Moseley's [21] cell (25-1280) in the international diffraction database for beta tantalum. ICDD 25-1280 was given a figure of merit $F30=5.9$ (0.076, 67), where 67 is the number of diffraction reflections possible for upto 30 observed reflections. In a 2002 paper, Arakcheeva [23] obtained single crystal beta tantalum from molten fluorides, and proposed a self-hosting complex beta tantalum structure ($a=1.0211$ nm, $c=0.53064$ nm, S.G. $P-42_1m$), following the σ -type Frank–Kasper structure [24,25].

In this investigation, tantalum coatings were sputter-deposited on the inner surfaces of A723 steel cylinders using a cylindrical magnetron, and steel and glass plates using a conventional and an in situ planar magnetron sputter system. Specimens with predominately beta tantalum contents were selected for analysis. We report on two forms of beta tantalum, one is highly (002) fiber-textured, and the other is more random oriented. For comparison with our experimental data, simulated diffraction patterns were generated using several structural models of beta tantalum. Stability of beta tantalum (002)-oriented grains, beta to alpha phase transformation, and hot hardness properties upon vacuum annealing were examined.

2. Experimental methods

A cylindrical magnetron system [9] was used to sputter the interior bore surface of A723 steel cylinders of 25–120 mm diameter. A conventional and an in situ [11,12] planar magnetron system were used to sputter tantalum on flat steel and glass plates of 2.54×3.81 cm². For the cylindrical sputter system, a cylindrical tantalum target, the cathode and the steel cylinders, the anode, were co-axial. Serial magnets accelerate electrons in a spiral motion around the cylinder longitudinal axis. Sputter gases were 99.999% pure argon or krypton; sputter target was 99.995% pure tantalum for all systems. In the annealing experiments, furnace and sample temperatures were recorded, vacuum anneal was performed to 900 °C at an interval of 50 °C, hold time was 25 min per anneal. Hot hardness measurements were performed using a Nikon hot harness tester.

Table 2 lists the deposition conditions and surface texture obtained for 12 specimens, ordered by sputter gas and gas pressure. In this paper, low-pressure specimens Kr1 and high-pressure specimen Kr5 are presented to show the difference between high (002)-textured vs. random beta tantalum. Data for low-pressure specimens Ar1 and high-pressure specimen Ar7 are presented to show phase transformation in high (002)-textured vs.

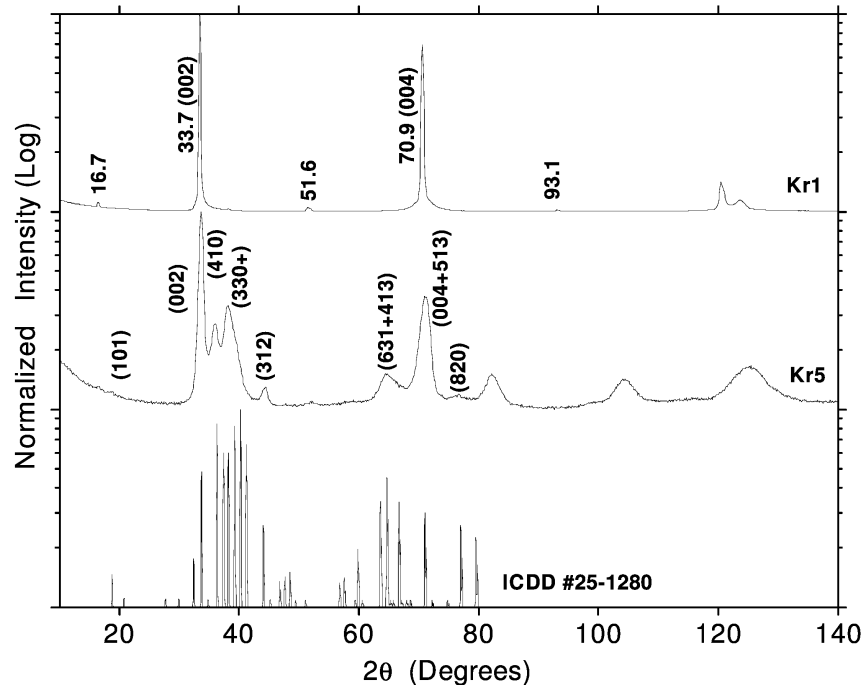


Fig. 1. XRD data for Kr1, deposited at 0.26 Pa (2 mTorr) and Kr5; deposited at 13 Pa (100 nTorr), compared to ICDD diffraction database for beta tantalum. Kr1 shows highly textured (002) beta tantalum, and Kr5 shows more randomly oriented (002) beta tantalum. Kr5 is in better agreement with ICDD database, due to its more random nature.

random beta tantalum. Hot hardness test was performed for specimen Ar1. XRD analysis was performed using a Scintag four-axis diffractometer, and a Bruker GADDS diffraction system, equipped with a Cu Göbel mirror and a two-dimensional detector for Debye diffraction cone analysis, and Cu $K\alpha$ radiation. In the GADDS system, Bragg–Brentano focusing geometry is no longer valid. Calibration of the system was made using NIST corundum standard.

3. XRD of random vs. highly textured (002) beta tantalum

Table 2 reveals that gas pressure is important in controlling texture in sputtered tantalum coatings. As pressure increases, the degree of surface texture decreases. In Fig. 1, XRD data are displayed for specimens Kr1, sputtered at 0.26 Pa (2 mTorr), Kr5, sputtered at 13 Pa (100 mTorr), and ICDD card 25-1280, which provides data up to $2\theta = 80^\circ$. The XRD patterns for Kr1 and Kr5 are distinctively different, Kr1 is highly (002) textured, while Kr5 is much more random.

Kr1 was a 14-h run on the Scintag; it showed strong peaks at 33.7° , 70.9° and weak peaks at 16.7° , 51.6° , 93.1° and peaks at 120.8° , 123.4° . Peak intensity ratio for $I_{16.7^\circ}/I_{33.7^\circ} = 0.0063$. ICDD 25-1280 lists a (513) peak at 71.096° , but not (004) peak. However, the observed peak at 70.9° is most likely attributed to beta tantalum (004) reflection at 70.9° . The three very weak

peaks at 16.7° , 51.6° and 93.1° fit locations of beta tantalum (001, 003, 005) reflections, as discussed in the structural simulation section. Alpha tantalum can exist in the specimen with negligible intensity. Diffraction peaks in the 120° – 124° region might be attributed to (006) reflection at 121.1° , residual alpha tantalum (321) reflection, or other beta tantalum lines. Kr5 was a 7-h run; it showed better agreement with ICDD 25-1280, due to its more random nature. The composite peak between 37° and 42° consist of (330, 202, 212, 411, 331) beta reflections. The broadened diffraction peaks, especially at higher 2θ angles, are difficult to interpret. Diffraction peak broadened are due to particle size and microstrain effects, and existence of composite peaks. The broadened peak at 71° showed a small shift towards higher 2θ , compared to the same peak in Kr1, demonstrating that the peak is likely due to contributions from both beta tantalum (004) and (513) reflections.

4. Texture in beta tantalum coatings

Debye diffraction cone is represented by 1024×1024 2θ vs. χ plots, where χ represents angle of specimen tilt. Random powder shows complete rings, and textured material shows incomplete rings. Fig. 2 gives sample Debye rings for Kr1 and Kr5, obtained as ω -scans at $2\theta = 30^\circ$ (left) and 75° (right). Kr1 is highly (002) textured, showing (002, 004) reflections, strong and broad textured composite peak (410, 330, 202, 212,

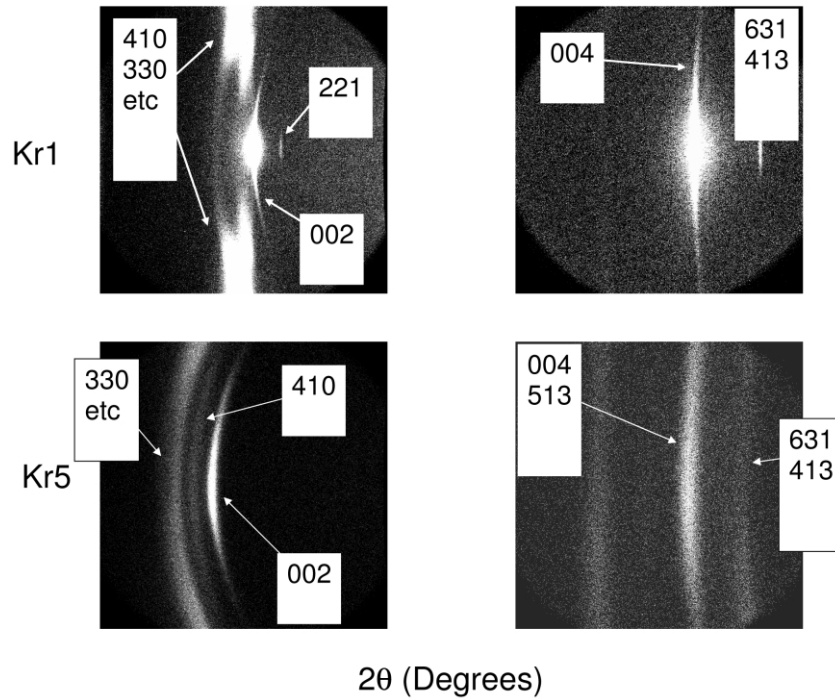


Fig. 2. Two-dimensional Debye diffraction rings for Kr1 and Kr5 at $2\theta = 30^\circ$ (left), and 75° (right) angles. Top row shows very highly textured Kr1, complicated texture and composite peaks. Bottom row shows more randomly oriented beta tantalum, and weak (002) texture in Kr5.

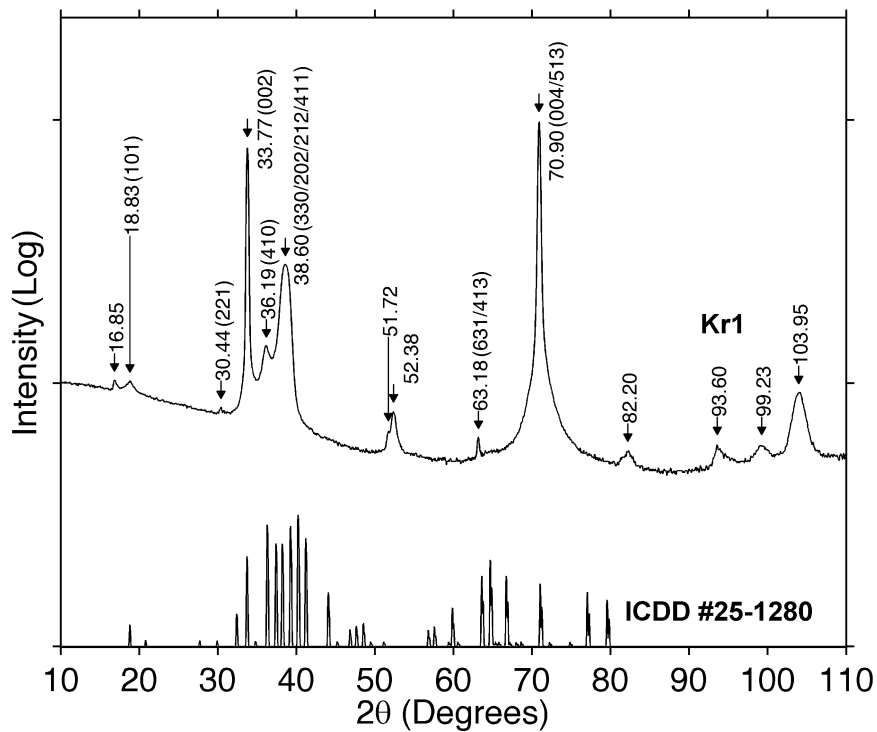


Fig. 3. Integrated XRD 2θ pattern for Kr1, summing over specimen tilt χ , compared to ICDD diffraction database for random beta tantalum. The major deviations are the strong (002), strong composite (004, 513) reflections, possible existence of the (00 l) reflection, and un-identified peaks as discussed in the text.

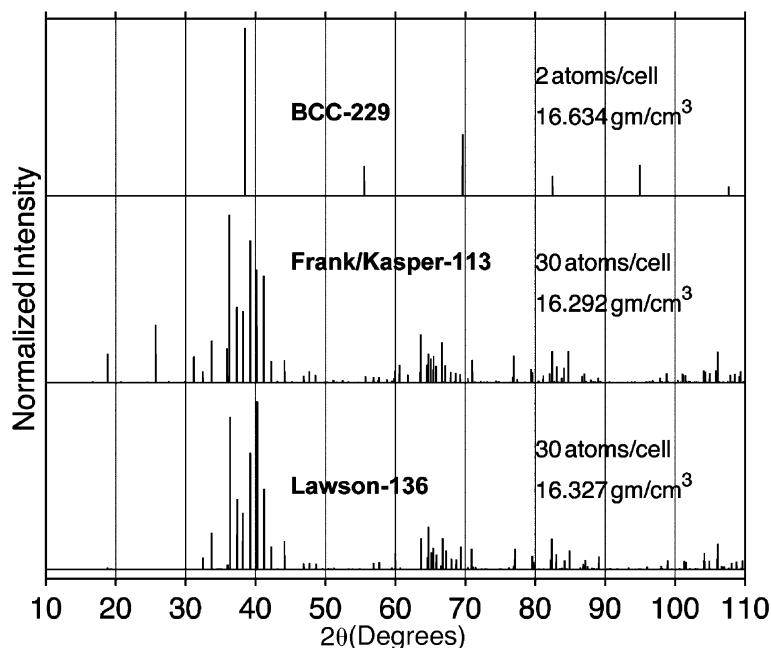


Fig. 4. Diffraction pattern simulation of alpha and beta tantalum, using atom locations and cell parameters for bcc alpha tantalum ($a=b=c=3.3058$ Å, S.G. IM3M), tetragonal beta tantalum using Lawson's model ($a=b=10.194$ Å, $c=5.313$ Å, S.G. $P42/mnm$) and Frank Kasper's model ($a=10.211$ Å, $c=5.3064$ Å, S.G. $P-42_1m$).

411, 331), and weaker (221, 631, 413) reflections. Kr5 shows more random beta tantalum, with some (002) texture. Again, the (004) peak was broadened, due to contribution from beta tantalum (513) reflection. Fig. 3 shows the integrated diffraction pattern for Kr1 compared to ICDD 25-1280. Our data show marginal agreement with ICDD 25-1280; major differences include very strong (002) reflection, strong (004) plus (513) composite peak at 71° , and weak peaks at 16.8° and 51.7° , and 93.6° . Two-dimensional integrated Kr1 looks very different from textured Kr1, but similar to more random Kr5 in Fig. 1. Read [18] also observed reflections at 16.6° and 52.2° , and indexed them as (100) and (301) reflections, using a tetragonal cell $a=0.534$ nm, $c=0.994$ nm. Pole figure data, not presented in this paper, showed the structure is consistent with a tetragonal cell $a=1.0194$ nm, $c=0.5313$ nm, and that Kr1 possesses strong (002) fiber-texture. Additionally, pole figures for 33.7° and 70.9° peaks showed a strong and sharp central pole. For 16.8° , 51.7° and 93.1° peaks, pole figures showed a strong and broader central pole.

5. Diffraction pattern simulation

Lattice constants and atom positions for bcc alpha tantalum $a=b=c=0.33058$ nm, S.G. IM3M [25], using two atoms per cell, for tetragonal beta tantalum cell ($a=b=1.0194$ nm, $c=0.5313$ nm, S.G. $P42/mnm$), [19–21] and an alternative tetragonal cell ($a=1.0211$ nm, $c=0.53064$ nm, S.G. $P-42_1m$) [23–25], using 30

atoms per cell were input into POWDERCELL [26] software to generate diffraction patterns for alpha and beta tantalum. Fig. 4 shows model calculations for diffraction pattern and density. The two patterns generated for beta tantalum are very similar. However, Lawson's 136, space group $P42/mnm$, is pseudo-symmetric, and allows only even (00 l), but not odd (00 l) reflections. The model predicts (002, 004, 513) reflections at 33.74° , 70.95° and 71.11° using Cu wavelength of 0.154178 nm. Frank–Kasper's 113, $P-42_1m$ structure, is non-centrosymmetric, allowing both even and odd (00 l) reflections. The model predicts (001, 002, 003, 004, 513, 005) reflections at 16.71° , 33.76° , 51.68° , 71.06° , 71.11° and 93.17° . The latter model is in better agreement with our data because it provides a possible interpretation for odd order (00 l) reflections.

6. Phase transformation in random (002) beta tantalum

Phase transformation property is important for tantalum applications in high temperature wear and erosion. Specimen Ar7 was cut from a cylinder with 45 mm diameter; it was subjected to anneal in vacuum to 850°C . Fig. 5 shows the diffraction patterns in linear scale, as deposited and after heated to 300, 650, 750 and 850°C . The baseline data showed more random beta tantalum. As the temperature increased, the (002) grains with fiber axis perpendicular to the specimen surface became very unstable. At 300°C , reduction of beta

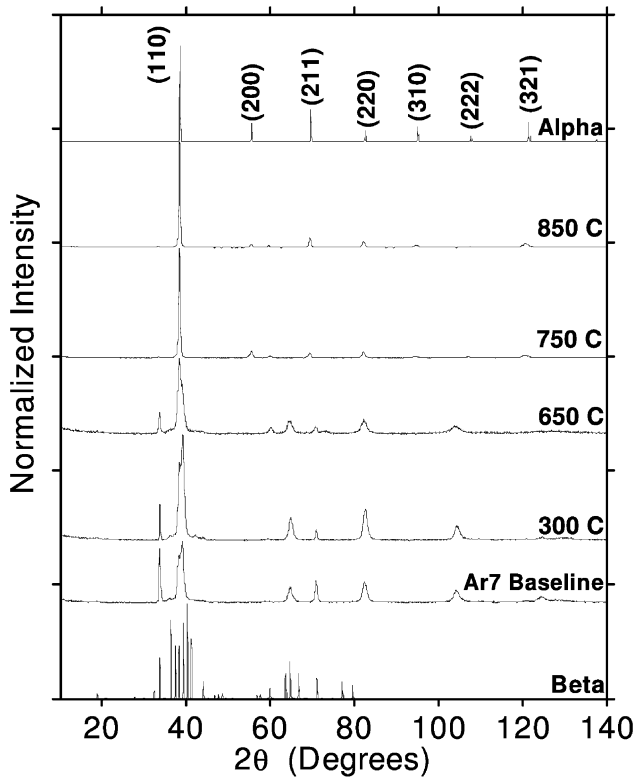


Fig. 5. Phase transformation behaviors of random beta tantalum Ar7 upon annealing. Beta phase tantalum transforms to bcc tantalum at 750 °C, resulting in (110) textured alpha tantalum.

tantalum (002) peak at 33.7°, and increase of the alpha tantalum (110) peak at 38.5° were observed. Complete alpha to beta tantalum transformation occurred near 750°. Further heating of alpha tantalum to 850° did not show further changes. The beta to alpha phase transformation resulted in a (110) textured alpha tantalum.

7. Phase transformation in highly (002) textured beta tantalum

Specimen Ar1 was deposited on a steel plate at 1.3 Pa (10 mTorr) in argon gas, resulting in highly (002) textured beta tantalum. The baseline data, compared to ICDD 25-1280 is shown in lower part of Fig. 7. The 30-min run showed three beta tantalum reflections, (002), (004) and (006), similar to Kr1. Fig. 6 shows the temperature dependence of hardness for (002) textured beta tantalum, using an alpha tantalum specimen for control. Upon annealing in vacuum, highly (002) textured beta tantalum hot hardness decreased from 1500 Vickers₅₀, to 400 Vickers₅₀. The drastic transition suggests a beta to alpha phase transformation near 300 °C. Upon annealing of an alpha tantalum specimen under the same temperature range, no hardness change was observed. Fig. 7 shows available XRD data in linear scale, as deposited, and at 100, 200 and 300 °C,

compared to ICDD alpha tantalum (04-0788) and beta tantalum (25-1280). Upon annealing, the (002) grains became unstable at low temperatures. We observed reduction of beta (002) intensity, recrystallization of beta (002) grains to form alpha tantalum (110), (211), (220) and (321) reflections at 100 and 200 °C. At 300 °C, beta to alpha phase transformation, re-orientation of the (002) grains to more random beta tantalum grains, and recrystallization to form nano-crystallites were observed. The 300 °C data showed possible oxidation of tantalum to form oxides.

8. Discussions

Not many recent papers have been published on beta tantalum addressing the texture and structure issues. Beta tantalum has been indexed as a tetragonal, a bcc based super-lattice structure with slight tetragonal distortions, and a hexagonal cell previously. ICDD [22] uses Moseley's cell [21] (25-1280) as international diffraction database for beta tantalum, but with a low figure of merit. Single crystal or single-phase random powder specimens should be used to make creditable structure determination. Our specimens may be impurity stabilized. However, we observed reflections, including even (00*l*) and possibly odd (00*l*) reflections. Our generated diffraction patterns show that non centrosymmetric $P-42_1m$ structure is similar to pseudo-symmetric $P4_2/mnm$ structure, but the former can provide better interpretation of data observed in this investigations. Our calculations show slightly higher density for 16.634 gm/cm³ in IM3M alpha tantalum, 16.327 gm/cm³ for $P4_2/mnm$ beta, and 16.292 gm/cm³ for $P-42_1m$

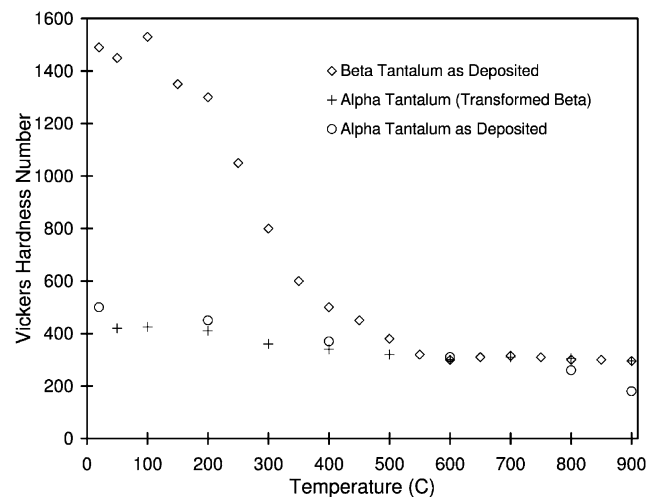


Fig. 6. Hot hardness measurements in highly (002) textured beta tantalum A1, and in alpha tantalum. The data show that hardness in alpha tantalum is insensitive to temperature changes. For Ar1, hardness in beta tantalum undergoes a drastic decrease near 250–350 °C, suggesting a phase transformation temperature near 300 °C.

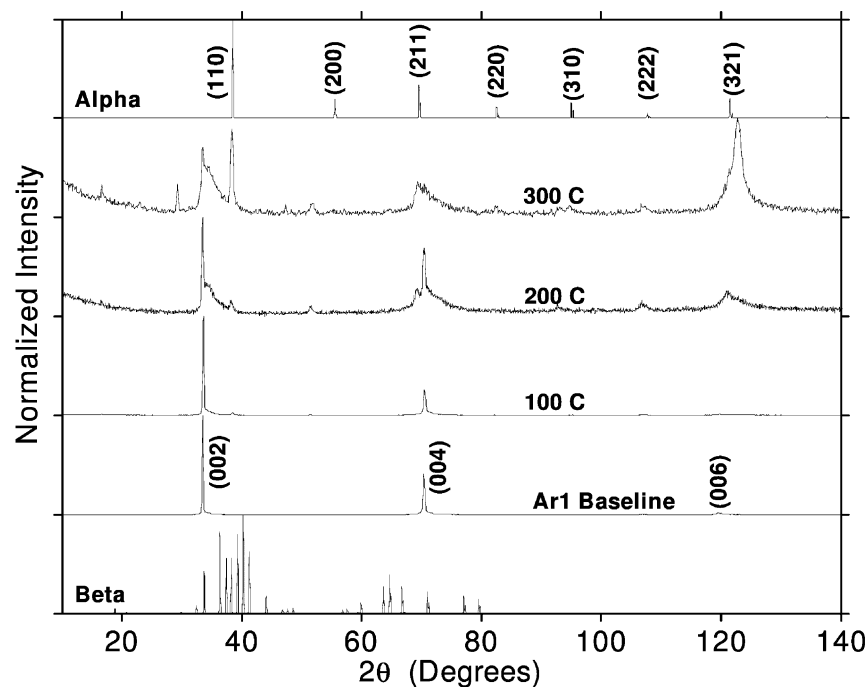


Fig. 7. In highly (002) fiber-textured beta tantalum Ar1, XRD showed unstable (002) grains at 100–300 °C. Partial phase transformation, re-orientation of the (002) grains, and re-crystallization to form fine-grained crystallites were observed.

beta tantalum. Dense coating with low porosity is most important for successful wear and erosion coatings.

Our annealing experiment of more random beta tantalum resulted in phase transformation near 750 °C, resulting in textured (110) alpha tantalum. This is in agreement with data quoted by Reed [18] and Hoogeveen [15]. Annealing experiment of highly textured beta tantalum revealed a reduction of hardness with temperature, suggesting a beta to alpha phase transformation at lower temperature. XRD data showed unstable (002) oriented grains at temperatures 100–300 °C. Additional XRD data at higher anneal temperatures are needed to establish phase transformation constraints for highly textured (002) beta tantalum.

The alpha tantalum coating demonstrated excellent high temperature wear and erosion prevention behavior [9,10]. However, sputter deposition generally produces a mixture of the beta and alpha tantalum phases. Sputtering parameters and interface materials are being studied to promote growth of the alpha phase [7,8]. Post anneal operation might be considered as an alternative method to produce all alpha tantalum coatings through phase transformation. Since highly textured (002) beta tantalum is thermally unstable at lower temperature compared to random beta tantalum, it may be more preferred for low temperature anneal.

9. Conclusion

Magnetron sputtering deposition produces two forms of beta tantalum coatings—one was highly (002) tex-

tured at lower sputter pressures, and the other was random (002) beta tantalum at higher pressures. At higher gas pressure, tantalum atoms suffer more collisions by the gas atoms and lost energy, resulting in more random oriented structure during nucleation and growth of the coatings. The two forms belong to the same tetragonal structure, but differ in the degree of texture. Structural calculations were made for alpha and beta tantalum to simulate diffraction patterns. Frank and Kasper [23–25] $P-42_1m$ structure is more compatible with our data, compared to Lawson and Donohue [19,20] $P42/mnm$ structure. Upon annealing, random beta tantalum showed phase transformation from beta to alpha tantalum near 750 °C, resulting in (110) textured alpha tantalum. Upon annealing, highly (002) textured beta tantalum showed drastic decrease in hardness, suggesting a beta to alpha phase transformation approximately 300 °C. Partial XRD data showed partial phase transformation, re-orientation of the (002) grains, and recrystallization to form fine-grained beta tantalum. Low temperature post-deposition anneal may be considered as a scheme to produce all alpha phase tantalum coatings, especially in highly textured (002) beta tantalum.

References

- [1] P. Catania, R.A. Roy, J.J. Cuomo, J. Appl. Phys. 74 (2) (1993) 1008.
- [2] K. Holloway, P.M. Fryer, Appl. Phys. Lett. 57 (17) (1990) 1736.

- [3] C. Cabral Jr., L.A. Clevenger, R.G. Schad, J. Vac. Sci. Technol. B 12 (4) (1994) 2818.
- [4] L.A. Clevenger, A. Mutscheller, J.M.E. Harper, C. Cabral Jr., K. Barmak, J. Appl. Phys. 72 (10) (1992) 4918.
- [5] K.M. Latt, Y.K. Lee, T. Osipowicz, H.S. Park, Mater. Sci. Eng. B 94 (2002) 111.
- [6] J.F. Cox, E.D. McClanahan, Proceedings of Tri-Service Gun Tube Wear and Erosion Symposium, (1982) 277.
- [7] D.W. Matson, E.D. McClanahan, E.D. Rice, S.L. Lee, D. Windover, Surf. Coat. Technol. 133–134 (2000) 411.
- [8] D.W. Matson, E.D. McClanahan, S.L. Lee, D. Windover, Surf. Coat. Technol. 146–147 (2001) 344.
- [9] S.L. Lee, M. Cipollo, D. Windover, C. Rickard, Surf. Coat. Technol. 120–121 (1999) 44.
- [10] S.L. Lee, D. Windover, M. Audino, D.W. Matson, E.D. McClanahan, Surf. Coat. Technol. 149 (2002) 62.
- [11] S.L. Lee, D. Windover, T.-M. Lu, M. Audino, Thin Solid Films 420–421 (2002) 287.
- [12] D. Windover, Ph.D. Dissertation, Rensselaer Polytechnic Institute (2002).
- [13] J.F. Whitacre, Ph.D. dissertation, University of Michigan (2000).
- [14] J.F. Whitacre, S.M. Yalisove, J.C. Bilello, Mat. Res. Soc. Symp. Proc. 562 (1999) 141.
- [15] R. Hoogeveen, M. Moske, H. Geisler, K. Samwer, Thin Solid Films 275 (1996) 230.
- [16] L. Liu, H. Gong, Y. Wang, J. Wang, A.T.S. Wee, R. Liu, Mater. Sci. Eng. C 16 (2001) 85.
- [17] P. Klaver, B. Thijsse, Thin Solid Films 413 (2002) 110.
- [18] M.H. Read, C. Altman, Appl. Phys. Lett. 7 (3) (1965) 51.
- [19] J. Donohue, H. Einspahr, Acta Cryst. B 27 (1971) 1740.
- [20] A.C. Lawson, C.E. Olsen, Acta Cryst. B 44 (1988) 89.
- [21] P.T. Moseley, C.J. Seabrook, Acta Cryst. B 29 (1973) 1170.
- [22] ICDD (International Centre for Diffraction Data) Database, (2002).
- [23] A. Arakcheeva, G. Chapuis, V. Grinevitch, Acta Cryst. B 58 (2002) 1.
- [24] F.C. Frank, J.S. Kasper, Acta Cryst. 11 (1958) 184.
- [25] F.C. Frank, J.S. Kasper, Acta Cryst. 12 (1959) 483.
- [26] G. Nolze, POWDERCELL software, (2003).